Harnessing Turing Instability through VO_2 Based Negative Feedback Loop Coupling System

Yanghao Wang[1], Pek Jun Tiw[1], Yaoyu Tao[2], Teng Zhang[1*] and Yuchao Yang[1,2,3,4*]
[1]School of Integrated Circuits, Peking University, Beijing 100871, China (*E-mail: tengzhang@pku.edu.cn, yuchaoyang@pku.edu.cn)
[2]Institute of Artificial Intelligence, Peking University, Beijing 100871, China.
[3]Guangdong Provincial Key Laboratory of In-Memory Computing Chips, School of Electronic and Computer Engineering, Peking University, Shenzhen 518055, China.
[4]Center for Brain Inspired Intelligence, Chinese Institute for Brain Research (CIBR), Beijing, 102206, China.

***Abstract*—This work proposes a novel coupling mechanism of VO_2 nonlinear oscillators based on the edge-of-chaos characteristic. Nonlinear oscillators are realized through the physical dynamics of Mott phase-change devices, and their collective behavior enables high speed and energy-efficient computation. The coupling of VO_2 devices is demonstrated through both experiments and simulations, revealing a novel operating principle based on Turing instability and negative feedback loop. Persistent oscillations are observed only with coupling, indicating edge-of-chaos behavior. Furthermore, a dynamic computing system coupling ten VO_2 devices is proposed for efficient encoding. The results demonstrate a speed of approximately 40 μs and a coupling energy of 2.24 μJ. This work advances the understanding of Turing instability-induced coupling coupling in physical systems, highlighting its advantages of high speed and energy efficiency, and its potential applications in unconventional computing.**

Keywords*—VO_2 devices, coupled oscillation, Turing instability, edge of chaos, dynamic computing

I. Introduction

The physical dynamics of solid-state electronic devices can be utilized as computing resources, like spin-torque devices [1] and Mott devices [2]. Among these, VO_2 Mott devices are of particular interest due to their high speed and low power insulator-to-metal phase transition dynamics occurring around 340 K [3]. This phenomenon arises from a temperature-sensitive electronic transition coupled with a structural transformation [4]. VO_2 devices exhibit volatile threshold resistance characteristics in quasi-static voltage scanning, making them suitable for constructing nonlinear oscillators with simple circuit configurations [5].

VO_2-based oscillators can mimic various neural activities and interact mutually through capacitive coupling, enabling massive parallelism and energy-efficient neuromorphic computing, with potential applications in associative memory [6], feature encoding [7], speech discrimination [8] and solving combinatorial problems [9]. From a circuit theory perspective, VO_2 Mott devices exhibit a local active characteristic, defined as their ability to amplify fluctuations and transition between working states according to external bias [10]. A physical device working within the local active and local stable region indicates a unique physical condition known as the 'edge of chaos' [11]. Theoretical memristors working at the edge of chaos can resolve the Hodgkin–Huxley 'all-or-none' mystery, the Turing instability, and the Smale paradox [12], which are widely present in our brains, but remain challenging to replicate with conventional devices.

In this work, we proposed a novel coupling mechanism of VO_2 nonlinear oscillators. As shown in Fig. 1a, VO_2 devices act as local active oscillators and show potential for emulating neural dynamics. When operating under certain bias conditions, individual oscillators exhibit no oscillation and only show stable attenuation dynamics. However, when oscillators are coupled, they exhibit persistent oscillations and synchronizing dynamics, corresponding to theoretical concepts of Turing instability and the Smale paradox [13]. Turing instability, which is the fundamental principle of self-organization in living systems, means steady-state dynamical systems may lose their steady state after the interaction, resulting in dynamic reaction systems that can never reach equilibrium [14]. This novel coupling effect is driven by negative feedback loop: the firing of one oscillator induces negative feedback on the other, triggering its critical threshold and propagating the oscillatory state back, resulting in sustained oscillatory behavior. We experimentally demonstrated and analyzed the coupling synchronization of two and three devices through this new coupling mechanism based on Turing instability. Furthermore, we explore scalability by designing a circuit-based implementation for expanded systems, as shown in Fig. 1b. The loop capacitance coupling VO_2 oscillators can be used for information encoding and encryption. Notably, uncoupled oscillators exhibit attenuation behavior and suppression of information (Fig. 1c), while coupling dynamic induces phase synchronization, where encoded information emerges (Fig. 1d).

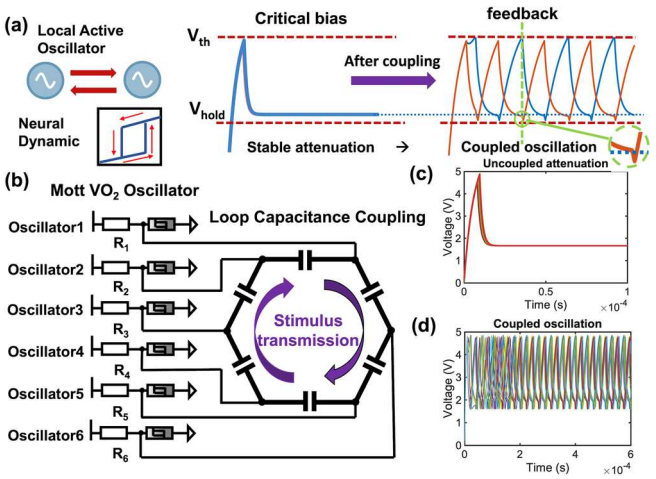

Fig. 1. Proposed VO_2 coupling mechanism. (a) Schematic of the negative feedback in two VO_2 local active oscillators. (b) Hardware implementation of VO_2 oscillators coupling system. (c) Attenuation behavior of uncoupled VO_2 oscillators. (d) Synchronous behavior of coupled VO_2 oscillators.

II. Single VO_2 Oscillator

We fabricated planar VO_2 threshold devices. The device's cross-sectional structure is illustrated in Fig. 2a, as observed under the transmission electron microscope (TEM). The

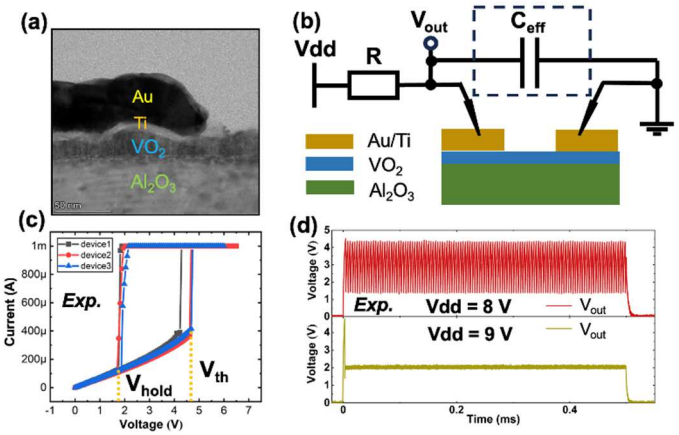

Fig. 2. Single VO_2 oscillator. (a) The TEM image of the VO_2 device. (b) The circuit diagram of a single VO_2 oscillator. (c) The quasi-static IV sweep of VO_2 devices. (d) The VO_2 oscillator's dynamic behaviors.

20 nm thick VO_2 films were grown on c-Al_2O_3 substrates in an epitaxial manner by pulsed-laser deposition technique. The electrodes, consisting of Ti (5 nm) and Au (40 nm), were patterned with electron beam lithography, followed by electron beam evaporation and lift-off, with an electrode spacing of 400 nm. Fig. 2b shows the circuit diagram of the single VO_2 oscillator. The effective parasitic capacitance C_{eff} originates from the VO_2 device and external cables. The VO_2 devices exhibit volatile threshold switching characteristics under quasi-static voltage sweep. Fig. 2c shows the hysteresis behavior of three VO_2 devices used in subsequent coupling experiments. Within the hysteresis, the devices transition from a high-resistance state (HRS) to a low-resistance state (LRS) when the applied voltage exceeds the threshold voltage (V_{th}). Conversely, when the voltage decreases below the hold voltage (V_{hold}), the devices revert to the high-resistance state. By applying different power supply voltages (V_{dd}) and series resistors (R), the device operates in different regimes, exhibiting either oscillatory or attenuation behavior [15]. In all experiments reported in this work, the series resistance R is fixed at 10 kohm. As shown in Fig. 2d, the VO_2 oscillator operates in two distinct regimes: oscillation occurs at $V_{dd} = 8$ V, while the device becomes stuck in the low resistance state at $V_{dd} = 9$ V. The effective parasitic capacitance C_{eff} is approximately 0.6 nF, with the following key device parameters: $V_{th} = 4.7$ V, $V_{hold} = 1.6$ V. The oscillatory behavior can be described by the following equation (1):

$$C_{\text{eff}}\frac{\mathrm{d}V_{out}}{\mathrm{d}t} = \frac{V_{\text{dd}} - V_{out}}{\mathrm{R}} - \frac{V_{out}}{R_{\text{VO}_2}} \tag{1}$$

III. Results of VO_2 Based Coupling System

Almost all previous studies on coupled oscillators require each oscillator to oscillate independently and exhibit intrinsic frequencies [16]. This principle forms the foundation of nearly all oscillator-based computing theories. However, this work reveals a novel path. When oscillators exhibit local active features, they can be biased at the critical stable regime but are able to oscillate through mutual triggering. The following experiments demonstrate this brand-new phenomenon.

A. Two coupled VO_2 oscillators

The circuit of two coupled VO_2 oscillators is shown in Fig. 3a, where the coupling capacitors C_o represent the strength of electrical interaction between two VO_2 oscillators. An

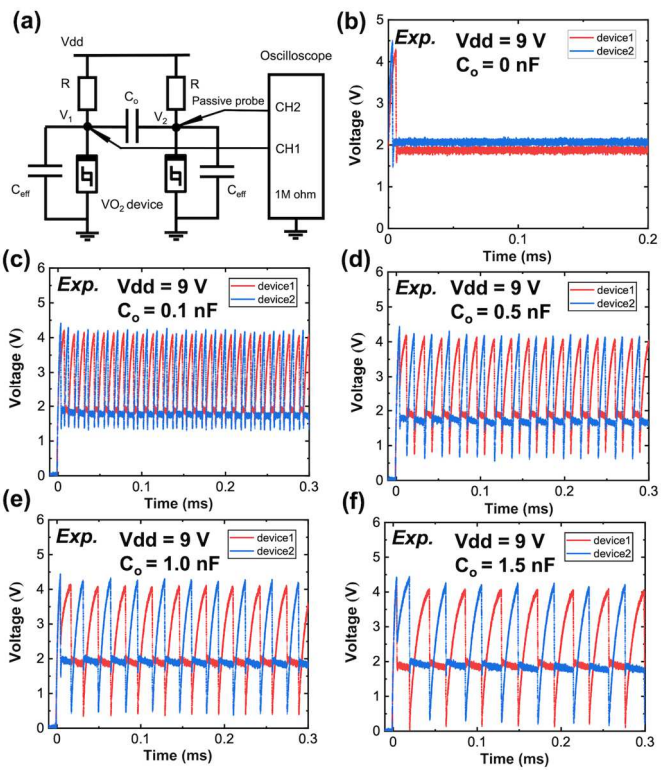

Fig. 3. Two coupled VO_2 oscillators based on Turing Instability. (a) The circuit diagram of two coupled VO_2 oscillators. (b) The attenuation behavior when two devices are not coupled. (c-f) The synchronous dynamic behaviors when two devices are coupled with the capacitance from 0.1 nF-1.5 nF.

oscilloscope with passive probes simultaneously monitors the voltage signals $V_1(t)$ and $V_2(t)$. In the experiments, V_{dd} was fixed at 9V and R at 10 kohm. As shown in Fig. 3b, neither VO_2 device oscillates in the absence of the coupling capacitor. However, when the coupling capacitor C_o is added, synchronous oscillation occurs in both the VO_2 oscillators. In this case, the oscillatory dynamic can be described by the following equation (2-3) :

$$C_{\text{eff}}\frac{\mathrm{d}V_1}{\mathrm{d}t} = \frac{V_{\text{dd}} - V_1}{\mathrm{R}} - \frac{V_1}{\mathrm{R}_{\text{VO}_2 1}} + C_{\text{o}}\frac{\mathrm{d}(V_2 - V_1)}{\mathrm{d}t} \tag{2}$$

$$C_{\text{eff}}\frac{\mathrm{d}V_2}{\mathrm{d}t} = \frac{V_{\text{dd}} - V_2}{\mathrm{R}} - \frac{V_2}{\mathrm{R}_{\text{VO}_2 2}} + C_{\text{o}}\frac{\mathrm{d}(V_1 - V_2)}{\mathrm{d}t} \tag{3}$$

Fig. 3c illustrates the oscillators' dynamic when $C_o = 0.1$ nF. The two oscillators exhibit oscillations of the same frequency but the opposite phase. The device-to-device variation will cause one oscillator to fire first. The firing of one oscillator causes the coupling capacitor to discharge, forcing the voltage of the other oscillator to drop to V_{hold}, thereby triggering its firing. The negative feedback, which typically suppresses the activity of conventional oscillators, stimulates the oscillators to sustain persistent oscillations in this case. As shown in Fig. 3d–f, the coupling oscillation behaviors are further investigated with C_o varying from 0.5 nF to 1.5 nF. As the coupling capacitance increases, the two oscillators consistently maintain opposite-phase synchronous oscillations, while the strength of their mutual interaction increases. Additionally, the frequency of these synchronous oscillations decreases gradually because of the increase of RC load in the circuit.

In phase space analysis, the state variable can be defined as the voltage across the effective parasitic capacitor. For dynamic computing systems, phase space contains more

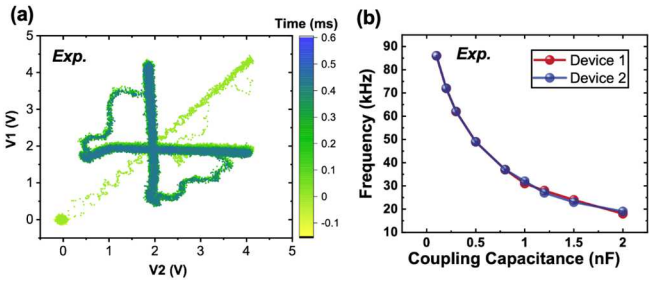

Fig. 4. The analysis of synchronization characteristics. (a) Butterfly-shaped phase space trajectory when the capacitance is 1.0 nF. (b) The relationship of oscillation frequency of two devices and coupling capacitance.

efficient and comprehensive information. Fig. 4a shows the continuous trajectory of the two coupled oscillators when C_o = 1 nF. Starting from the initial state, the trajectory converges onto a butterfly-shaped limit cycle, which is independent of the initial phase. Therefore, this novel coupling mechanism can form a stable limit cycle trajectory. Fig. 4b depicts the relationship between the oscillating frequency of the two coupled oscillators and the coupling capacitance. The coupling capacitance determines the frequency of the coupled oscillations. When the coupling capacitance is large, the mutual interaction is stronger, which makes the synchronization behavior more difficult to converge. Consequently, there is a small deviation in frequency when the coupling capacitance exceeds 1 nF.

B. Three coupled VO_2 oscillators

To further explore the coupling dynamic, we constructed a circuit of three coupled oscillators, as shown in Fig. 5a. In this case, the coupling capacitors form a closed ring structure, completing the negative feedback loop and improving synchronization convergence.

We fixed V_{dd} at 9 V to ensure that the oscillators cannot oscillate spontaneously. We used the Fast Fourier Transformation (FFT) to verify the synchronization frequency of the oscillators. The result is shown in Fig. 5b. The synchronous frequency is 139.1 kHz. As shown in Fig. 5c, when the coupling capacitance is 0.2 nF, the three devices oscillate with a 120-degree phase difference between each pair. The limit-cycle trajectory of the coupled VO_2 oscillators in the 3-dimensional phase plane further demonstrates the synchronous feature, as shown in Fig. 5d. The trajectory projection on each coordinate plane presents a box-like shape.

C. Phase encoding in dynamic computing

In a computing system based on coupling oscillation, information is encoded by phase or frequency. Under this Turing Instability coupling mechanism, the oscillators do not exhibit intrinsic frequency but instead synchronize to a unified oscillation frequency, making them particularly suitable for phase encoding. The general coupled oscillator model function [7] is shown in equation (4)

$$\sum_j C_{ij}\frac{dV_i}{dt} - \sum_{j\neq i} C_{ij}\frac{dV_j}{dt} = \frac{V_{dd}-V_i}{R_0} - \frac{V_i}{R_{VO_2 i}} \qquad (4)$$

We propose a dynamic computing module consisting of multiple oscillators and a "key" for accessing this computing module. Without the key, the coupling loop is incomplete, resulting in either attenuated dynamics or unsynchronized oscillations among the oscillators. When the key is inserted, the loop is completed, and phase information emerges in the

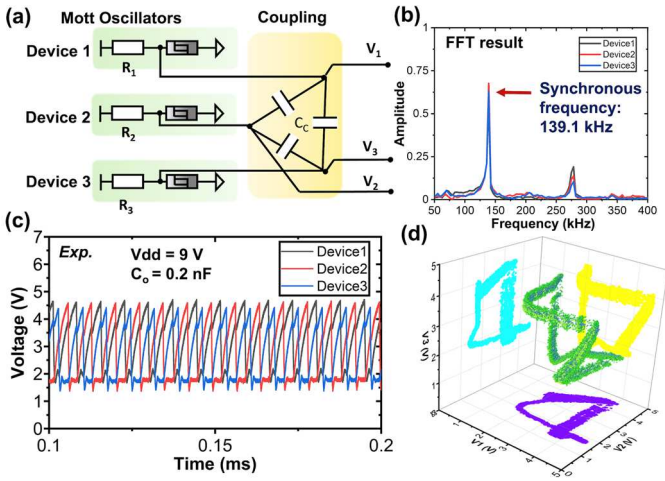

Fig. 5. Three coupled VO_2 oscillators based on Turing Instability. (a) The circuit diagram of three coupled oscillators. (b) The Fast Fourier Transform of the oscillation behaviors. (c) The synchronous dynamic behaviors when coupling capacitances are all 0.2 nF. (d) The limit cycle phase space trajectory of the three oscillators.

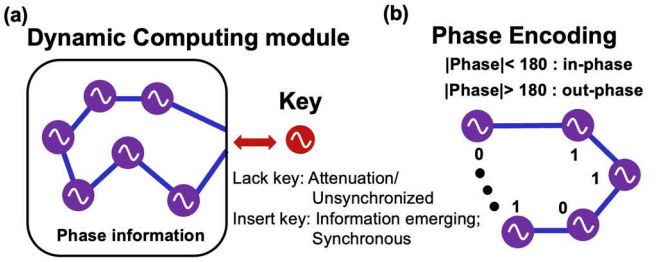

Fig. 6. Schematic of dynamic computing based on local active oscillators. (a) The physical encryption applications with Turing Instability. (b) The binarization phase encoding in the coupling loop.

system as all oscillators achieve synchronization, as shown in Fig. 6a.

Binary phase encoding can effectively mitigate the impact of cycle-to-cycle variation. We designate oscillator 1 as the reference and keep it represented as phase '0', and all other oscillators' phases are defined by:

If the |Phase|<180, it is in-phase and can be defined as '0'.

If the |Phase|>180, it is out-of-phase and can be defined as '1'.

This enables a system of n oscillators to encode 2^{n-1} distinct states, as shown in Fig. 6b.

In a physical encryption application, 10 VO_2 devices have device-to-device variations, and we selected one device as a key and the other nine devices as computing modules. The physical variations decided their phase relationship after synchronization, which can be encoded as ten-bit information. If we bias the device on the self-oscillation region, all the information can be read directly, and the coupling behavior can be predicted. However, if we bias the device on the critical bias on which they only behave in a decay dynamic. Therefore, reading the single oscillator cannot get all the physical device's information. Coupling the 9 devices in the computing module will cause unsynchronized oscillation. Only when using the key oscillator to couple with a loop, the phenomenon of synchronization will happen and information will emerge in the phase difference.

In the simulation, we set a small range (0.1 V) of device-to-device variation, and the initial voltage of each oscillator is uniformly distributed between 0-1 V. The coupling capacitance is 0.1 nF. As shown in Fig. 7a, without the key,

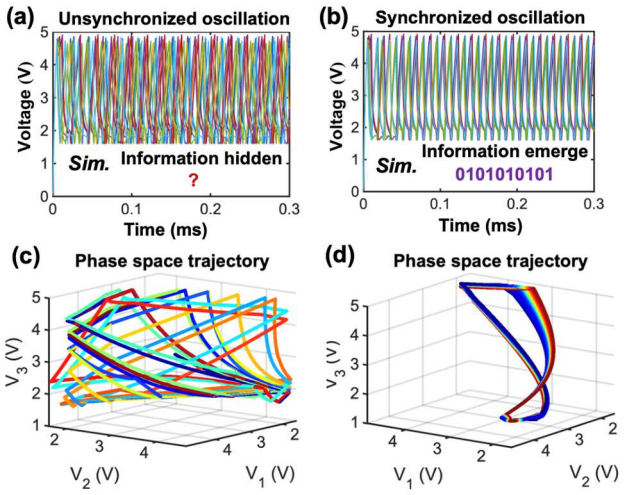

Fig. 7. Ten VO_2 oscillators for physical encryption. (a) The asynchronous oscillation when the key VO_2 oscillators are uncoupled. (b) The synchronous oscillation when coupled. (c) The chaotic phase space trajectory of uncoupled situation. (d) The limit cycle trajectory of coupled situation.

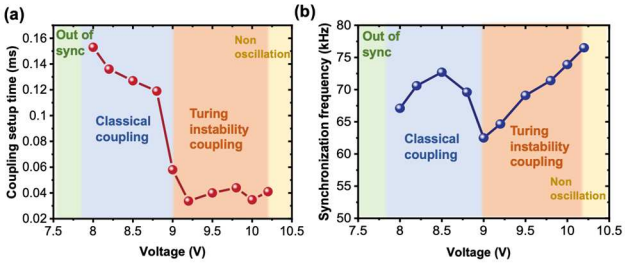

Fig. 8. The comparison with classical coupling. (a) The relationship between coupling setup time and voltage supply. (b) The relationship between synchronization frequency and voltage supply.

the oscillators fail to synchronize. However, when the key is inserted, the oscillators form a feedback loop and achieve synchronization, as shown in Fig. 7b. The trajectory in phase space further validates these results. As shown in Fig. 7c, the oscillators are not synchronized without the key, while Fig. 7d demonstrates that the oscillators' trajectory falls on a limit-cycle. It can serve as a physical ID to a dynamic computing system. The coupling energy consumption is 2.24 μJ.

We further studied the difference between the two types of coupling mechanisms. The first is the classical coupling method, where the oscillator has an intrinsic frequency. The other is the Turing instability coupling, in which oscillators can only oscillate when coupled. Fig. 8a shows that the coupling setup time for Turing instability coupling is approximately 40 μs, indicating that this mechanism converges faster and provides greater robustness. As shown in Fig. 8b, the synchronization frequency ranges from 62 kHz to 77 kHz. The frequency will briefly decrease during mechanism switching, and then monotonically increase as the supply voltage rises until the VO_2 oscillators cannot oscillate through any mechanism. The energy-delay product of classical coupling is 565.9 pJs under V_{dd} = 8 V, while the Turing instability is only 22.6 pJs under V_{dd} = 9 V due to fast coupling convergence speed.

IV. Conclusion

This work proposes a physically intuitive explanation and implementation scheme for hardware Turing Instability coupling. Through both experiments and simulations, we demonstrate that a negative feedback loop can construct coupling, transforming the oscillators from a "dying" state to an "active" state. The new coupling mechanism offers faster convergence and an intrinsic information-hiding function, which holds great potential for dynamic computing based on nonlinear physical dynamics in solid-state electronic devices.

Acknowledgment

This work was supported by the National Natural Science Foundation of China (61925401, 61927901, 92164302, 8206100486 and 62404007), Beijing Natural Science Foundation (L234026, 25D40029, 25FY3314) and the 111 Project (B18001).

References

[1] J. Grollier, D. Querlioz, K. Y. Camsari, K. Everschor-Sitte, S. Fukami, and M. D. Stiles, 'Neuromorphic spintronics', *Nat. Electron.*, vol. 3, no. 7, Art. no. 7, 2020, doi: 10.1038/s41928-019-0360-9.

[2] S. Kumar, R. S. Williams, and Z. Wang, 'Third-order nanocircuit elements for neuromorphic engineering', *Nature*, vol. 585, no. 7826, pp. 518–523, 2020, doi: 10.1038/s41586-020-2735-5.

[3] Y. Zhou and S. Ramanathan, 'Mott Memory and Neuromorphic Devices', *Proc. IEEE*, vol. 103, no. 8, pp. 1289–1310, 2015, doi: 10.1109/JPROC.2015.2431914.

[4] K. Martens et al., 'Field Effect and Strongly Localized Carriers in the Metal-Insulator Transition Material VO_2', *Phys. Rev. Lett.*, vol. 115, no. 19, p. 196401, 2015, doi: 10.1103/PhysRevLett.115.196401.

[5] O. Maher et al., 'Implementation of FitzHugh-Nagumo Neurons using Nanoscale VO_2 Devices', in *2024 IEEE European Solid-State Electronics Research Conference (ESSERC)*, 2024, pp. 729–732. doi: 10.1109/ESSERC62670.2024.10719575.

[6] N. Shukla et al., 'Pairwise coupled hybrid vanadium dioxide-MOSFET (HVFET) oscillators for non-boolean associative computing', in *2014 IEEE International Electron Devices Meeting (IEDM)*, 2014, p. 28.7.1-28.7.4. doi: 10.1109/IEDM.2014.7047129.

[7] K. Yang et al., 'High-order sensory processing nanocircuit based on coupled VO_2 oscillators', *Nat. Commun.*, vol. 15, no. 1, p. 1693, 2024, doi: 10.1038/s41467-024-45992-8.

[8] S. Dutta, A. Khanna, W. Chakraborty, J. Gomez, S. Joshi, and S. Datta, 'Spoken vowel classification using synchronization of phase transition nano-oscillators', in *2019 Symposium on VLSI Technology*, 2019, pp. T128–T129. doi: 10.23919/VLSIT.2019.8776534.

[9] O. Maher et al., 'A CMOS-compatible oscillation-based VO2 Ising machine solver', *Nat. Commun.*, vol. 15, no. 1, p. 3334, 2024, doi: 10.1038/s41467-024-47642-5.

[10] T. D. Brown, S. Kumar, and R. S. Williams, 'Physics-based compact modeling of electro-thermal memristors: Negative differential resistance, local activity, and non-local dynamical bifurcations', *Appl. Phys. Rev.*, vol. 9, no. 1, p. 011308, 2022, doi: 10.1063/5.0070558.

[11] L. Chua, 'Memristor, Hodgkin–Huxley, and Edge of Chaos', *Nanotechnology*, vol. 24, no. 38, p. 383001, 2013, doi: 10.1088/0957-4484/24/38/383001.

[12] L. O. Chua, 'Memristors on "edge of chaos"', *Nat. Rev. Electr. Eng.*, vol. 1, no. 9, pp. 614–627, 2024, doi: 10.1038/s44287-024-00082-1.

[13] A. Ascoli, A. S. Demirkol, R. Tetzlaff, and L. Chua, 'Edge of Chaos Theory Resolves Smale Paradox', *IEEE Trans. Circuits Syst. Regul. Pap.*, vol. 69, no. 3, pp. 1252–1265, 2022, doi: 10.1109/TCSI.2021.3133627.

[14] A. M. Turing, 'The chemical basis of morphogenesis', *Philos. Trans. R. Soc. Lond. B. Biol. Sci.*, vol. 237, no. 641, pp. 37–72, 1952, doi: 10.1098/rstb.1952.0012.

[15] P. Maffezzoni, L. Daniel, N. Shukla, S. Datta, and A. Raychowdhury, 'Modeling and Simulation of Vanadium Dioxide Relaxation Oscillators', *IEEE Trans. Circuits Syst. Regul. Pap.*, vol. 62, no. 9, pp. 2207–2215, 2015, doi: 10.1109/TCSI.2015.2452332.

[16] G. Csaba and W. Porod, 'Coupled oscillators for computing: A review and perspective', *Appl. Phys. Rev.*, vol. 7, no. 1, p. 011302, 2020, doi: 10.1063/1.5120412